Solid Freeform Fabrication 2023: Proceedings of the 34th Annual International Solid Freeform Fabrication Symposium – An Additive Manufacturing Conference
Reviewed Paper

Effects of Build Orientation and Heat Treatment on the Porosity Distribution and Morphology within Inconel 625 Fabricated via Laser Powder Bed Fusion

Mohanish Andurkar[1], Bart Prorok[2], John Gahl[3], Scott Thompson[4,*]

[1] Alan Levin Department of Mechanical and Nuclear Engineering, Kansas State University, Manhattan, KS 66506, United States of America.

[2] Department of Materials Engineering, Auburn University, Auburn, AL 36849, United States of America.

[3]Department of Electrical and Computer Engineering and University of Missouri Research Reactor (MURR), University of Missouri, Columbia, Missouri, 65211, United States of America.

[4]Department of Mechanical and Aerospace Engineering and University of Missouri Research Reactor (MURR), University of Missouri, Columbia, MO 65211, United States of America.

*Corresponding author: smthompson@missouri.edu

Abstract

The effects of build orientation, i.e., vertical, or diagonal (45º), and heat treatment on the porosity characteristics within Inconel 625 (IN625) fabricated via laser powder bed fusion (L-PBF) was experimentally investigated. Selected samples were heat treated at 1050 ℃ for 1-hour to promote evolution of pores. X-Ray Computed Tomography (XCT) was performed on samples to generate three-dimensional porosity maps. Volume Graphics (VG) software was used to inspect and quantify porosity distributions. Results indicate that build orientation and heat treatment influence measured porosity count. As-built (no heat treatment) sample microstructure was observed to have lower porosity count when compared to heat-treated samples. The vertically built sample was observed to have lower porosity relative to its diagonally built counterpart. The porosity morphology or diameter was observed to vary after heat treatment. On the other hand, the sphericity of pores was not affected by different build orientation and heat treatment.

Keywords: laser powder bed fusion, X-ray CT, porosity measurements, pore morphology

Introduction

Additive manufacturing (AM) continues to revolutionize how industry designs, manufactures, and distributes components to end users. AM is versatile, flexible, highly customizable and, as such, has gained significant interest from academics and various industries. AM offers opportunities to build complex geometry parts with no additional tooling, reduction of process costs and potential to achieve zero waste manufacturing by maximizing material utilization, better control over the building process, on-demand manufacturing, and more [1]. Despite these capabilities of AM, its wide application for 'printing' high-value metal parts is currently restrained due to such parts having some level of microstructural defects such as porosity, voids, and residual stress. These defects can significantly degrade the structural integrity and performance of final components. Accurate detection, characterization, and prediction of these defects and irregularities have an important and immediate impact in the AM of fully dense parts [2]. ISO/ASTM 52900:2021 standard describes seven categories of AM. Powder bed fusion (PBF) is more accepted in industries due to several advantages it offers such as low cost, minimal support

structure requirements as the powder bed itself provides supports, larger material library, and the capability to recycle the unused powder [3].

Porosity is defined as the ratio total pore volume to bulk material volume. Porosity can be considered as the Achilles heel of AM. Defect quantification and mitigation techniques have been an active research area in the metals AM field. Quantification of defects such as porosity in AM can be performed using x-ray computed tomography (XCT). XCT provides 3D information on internal defects by the reconstruction of a series of radiographs taken as the sample rotates over 180º or 360º [4]. The XCT technique is a widely applicable, powerful, and nondestructive inspection approach to evaluate and analyze geometrical and physical characteristics of materials, especially internal structures, and feature [5]. XCT has been used to characterize the size, shape, and volume of the pores in the sample. In the past, XCT analysis was used to correlate with process parameters used during the print to generate different porosity in parts [6]. A. Du Plessis provided a summary of pore types in AM metals [7]. Along with quantification, mitigation of these defects is equally critical to enhance the performance of the end user part. To minimize porosity in AM metals, it is important to carefully control the printing process. This can be done by adjusting the laser power [8], [9], using high-quality metal powder [10], build orientation [11], and carefully selecting the printing parameters [12]. Post-processing techniques such as hot isostatic pressing (HIP) can also be used to reduce porosity and improve the mechanical properties of the final product. Although these studies were focused on varied materials, the porosity evolution in AM Inconel 625 (IN625) still needs to be comprehended in detail.

The aim of this study is to investigate the effects of L-PBF build orientation and post-processing heat treatment on the porosity count, pore diameter, and sphericity in L-PBF IN625 samples. 3D porosity maps obtained via XCT technology will be provided. The goal is to provide a deeper understanding of the relationships between build orientation, heat treatment and porosity which should help in determining optimized process parameters for manufacturing highly dense components via L-PBF and subsequent heat treatments.

Experimental Methods

AM IN625 cube samples were fabricated in a Concept Laser MLab 100R system. The printing was conducted in an argon atmosphere. An iterative method was used to determine optimized process parameters to print nearly full dense samples. The detailed optimize process parameters, scan strategy, powder composition used to print samples is explained in the study conducted previously [13]. Vertically and diagonally printed samples in the as-built and 1050 ℃- 1-hour heat treated condition were inspected. All samples were heat treated using a heating ramp of ~5℃/min and later air cooled in the furnace. The uncertainty in heat treatment temperatures is ± 5 ºC. The rationale behind using this heat treatment schedule was to investigate the effect of elevated temperature on the pore characteristics such as frequency, size, and sphericity.

Porosity in a 3D XCT scan is identified as a low-density area (i.e., void space / air bubble) surrounded by higher density material. Raw XCT scan data for the part was reviewed and the region of interest to be analyzed was established and adjusted parameters which are used to define the pores. This parameter tuning phase increases the accuracy of both identification and quantification of each pore. A wealth of pore attribute data is calculated for each pore and includes pore count, size, and sphericity.

Porosity maps and statistics were measured using a NSI X5000 225 XCT system available at Delphi Precision Imaging Corporation (Redmond, WA USA). Sample part dimensions were approximately 5 mm x 5 mm x 10 mm in size. Samples were mounted on a rotating stage and

imaged using 255 kV and 160 μA with 0.25 mm of copper (Cu) filter for beam hardening. A total of 5600 projections were taken using an oversampled sub-pixel scan technique with 5 integrated frames yielding a voxel size of 15 μm. 3D XCT reconstruction was done with NSI EFX software; Analysis / Visualization was performed using commercial software VGSTUDIO MAX 2022 (Volume Graphic, Heidelberg, Germany). Porosity results can be visualized in the 3D CT scan model/2D slice views and individually color coded based on volume or other chosen attributes. This pore list can then be sorted and/or filtered based on a variety of attributes and can be exported as tabular data. The certainty of detected pores truly being gas pores (and not an artifact, surface void, inclusion, etc.) was set to be greater than or equal to 1 in the software. This ensured more accurate detection of pores with lighter gray contrast which indicates presence of gas. This study only focuses on the gas-entrapped pores and its quantitative analysis occurring in the microstructure of all samples.

Results

Figure 1 shows the total porosity count in all samples. The total porosity count in as-built vertical (V), diagonal (D), heat treated vertical, and diagonal samples are 186, 367, 1117, 1389, respectively. The as-built vertically printed sample has a lower porosity count compared to diagonally printed sample. This may be due to the presence of different heat transfer paths involving conduction between adjacent powder layers and Marangoni convention. The difference in the thermal conductivity between layers oriented in vertical and diagonal directions also has influenced different porosity levels in the samples. 3D porosity maps of vertically and diagonally printed as-built and 1050 ℃- 1-hour heat treated IN625 samples are presented in Figures 2 and 3. As seen in Figs 2 and 3., there is a considerable influence of build orientation and heat treatment on the porosity counts in the AM IN625 samples.

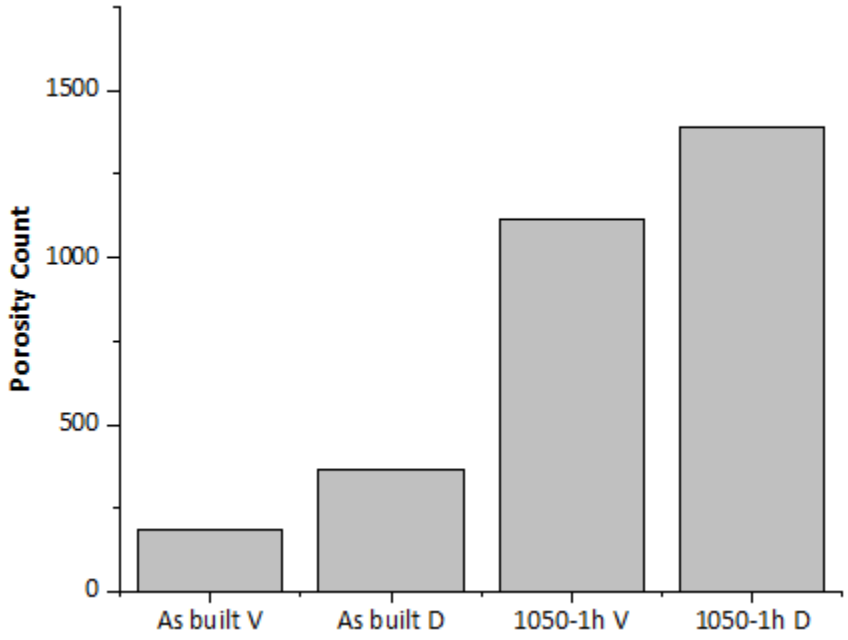

Fig 1. Porosity count in as-built vertical (V), as-built diagonal (D), 1050 ℃- 1h heat treated vertical printed, and 1050 ℃- 1h heat treated diagonal printed IN625 samples.

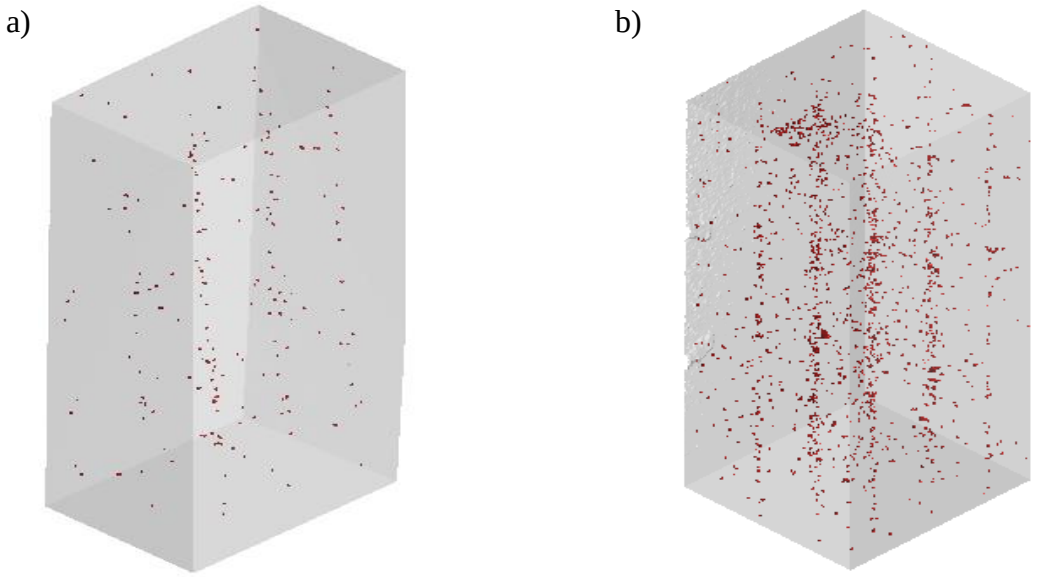

Fig 2. Porosity maps of a) as-built vertical and b) 1050 ℃- 1h heat treated vertical printed AM IN625 samples. Red points represented pores.

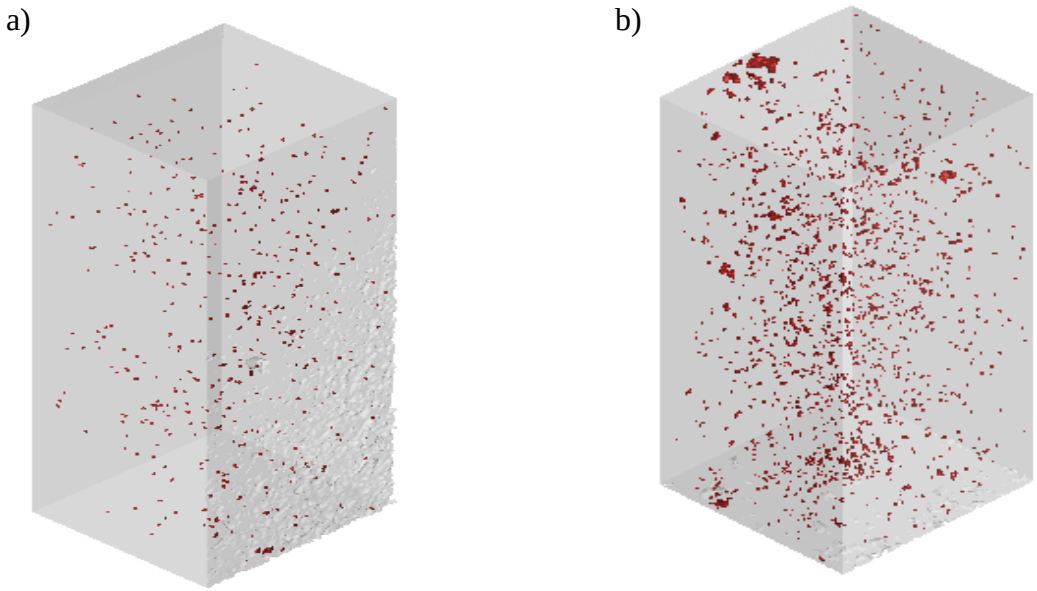

Fig 3. Porosity maps of a) as-built diagonal and b) 1050 ℃- 1h heat treated diagonal printed AM IN625 samples. Red points represented pores.

Pore diameter distribution found within as-built and 1050 ℃- 1-hour heat treated vertically printed samples is presented in Figure 4. Post 1050 ℃- 1-hour heat treatment, the pore diameters in the vertically printed samples were observed to increase. The average pore diameter for the as-built and 1050 ℃- 1-hour heat treated vertical samples are 60.226 ± 10 and 67.35 ± 10.2 μm, respectively. The formation of pores and the increased pore diameter due to heat treatment

presumably resulted from the temperature-driven equilibrium diffusion and increase gas (argon) pressure inside of the pores. Similar observations were reported in previous studies [14], [15].

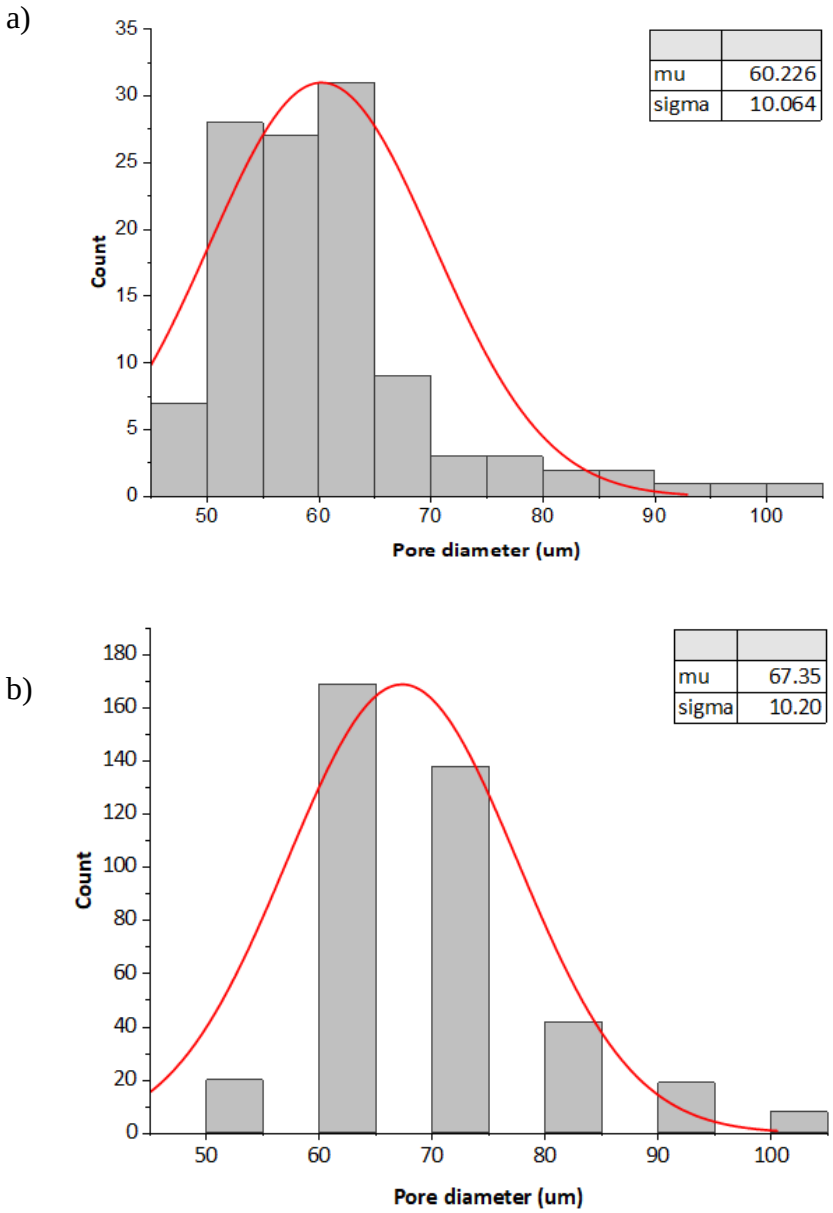

Fig 4. Pore diameter distribution (in μm) in a) as-built vertical and b) 1050 ℃- 1-hour heat treated vertical printed AM IN625 samples. Average and standard deviation are represented with mu and sigma values, respectively.

Pore diameter distribution found within as-built and 1050 ℃- 1-hour heat treated diagonally printed sample is presented in Figure 5. A similar trend compared to vertically printed samples was observed in the diagonally printed samples. The average pore diameter for the as-built and 1050 ℃- 1-hour heat treated diagonal samples are 59 $\pm$ 8.13 and 68.48 $\pm$ 10.59 μm respectively. This indicates regardless of build orientation, heat treatment resulted in the expansion of the pores. In addition, it can be observed that pore diameter distribution in the as-built vertically and diagonally samples showed very slight variation in the average pore diameter value, indicating

minimal effect of the build orientation on the average pore diameter. This is indicated by the similarity in the mu values shown in Figures 4 and 5.

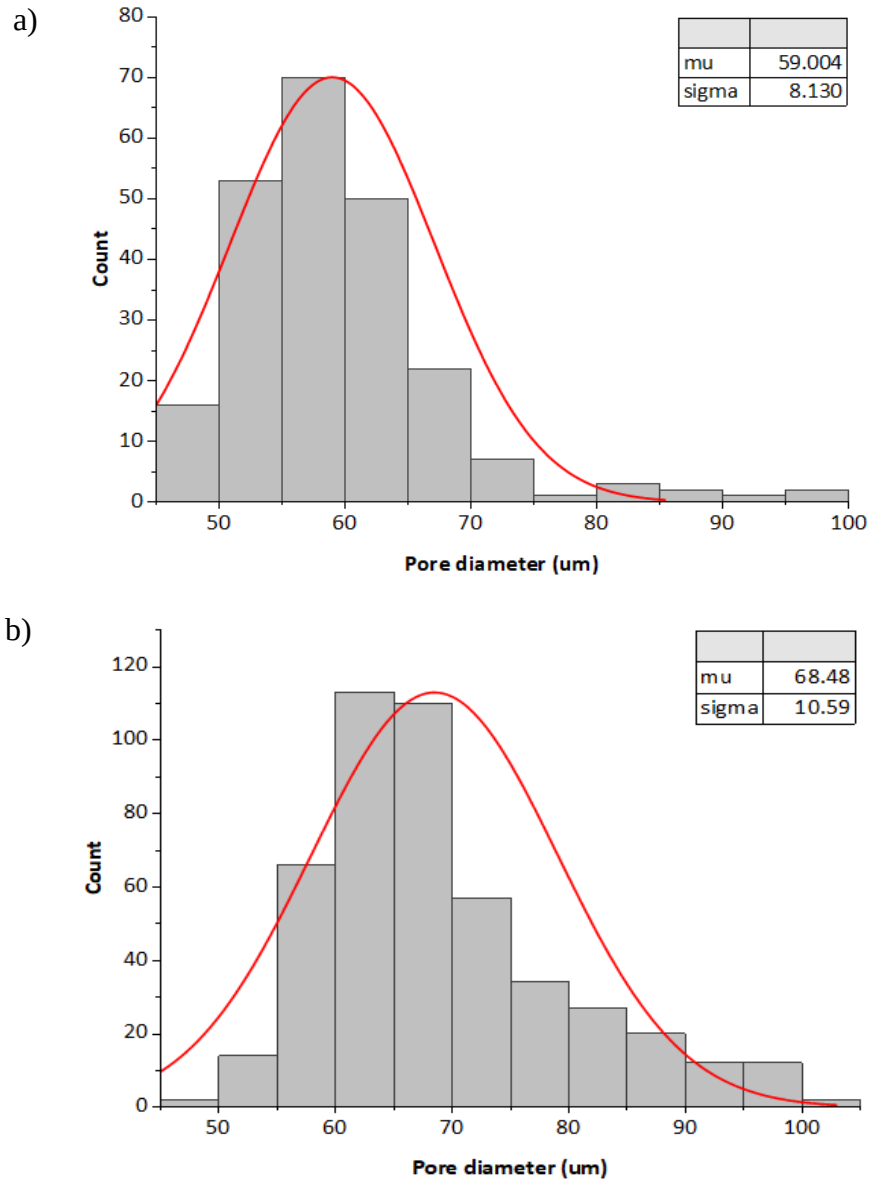

Fig 5. Pore diameter distribution (in μm) in a) as-built diagonal and b) 1050 ℃- 1-hour heat treated diagonal printed AM IN625 samples. Average and standard deviation are represented with mu and sigma values, respectively.

Pore sphericity within the as-built and 1050 ℃- 1-hour heat treated vertically printed samples is presented in Figure 6. As presented in Fig. 6., the effect of heat treatment on the sphericity of the pores is not noticeable at all. The average pore sphericity in the as-built and 1050 ℃- 1-hour heat treated vertically built samples are 0.94 $\pm$ 0.2. The mu and sigma values in Figs. 6 and 7 represent average and standard deviation values. The red curve represents the distribution curve of the data.

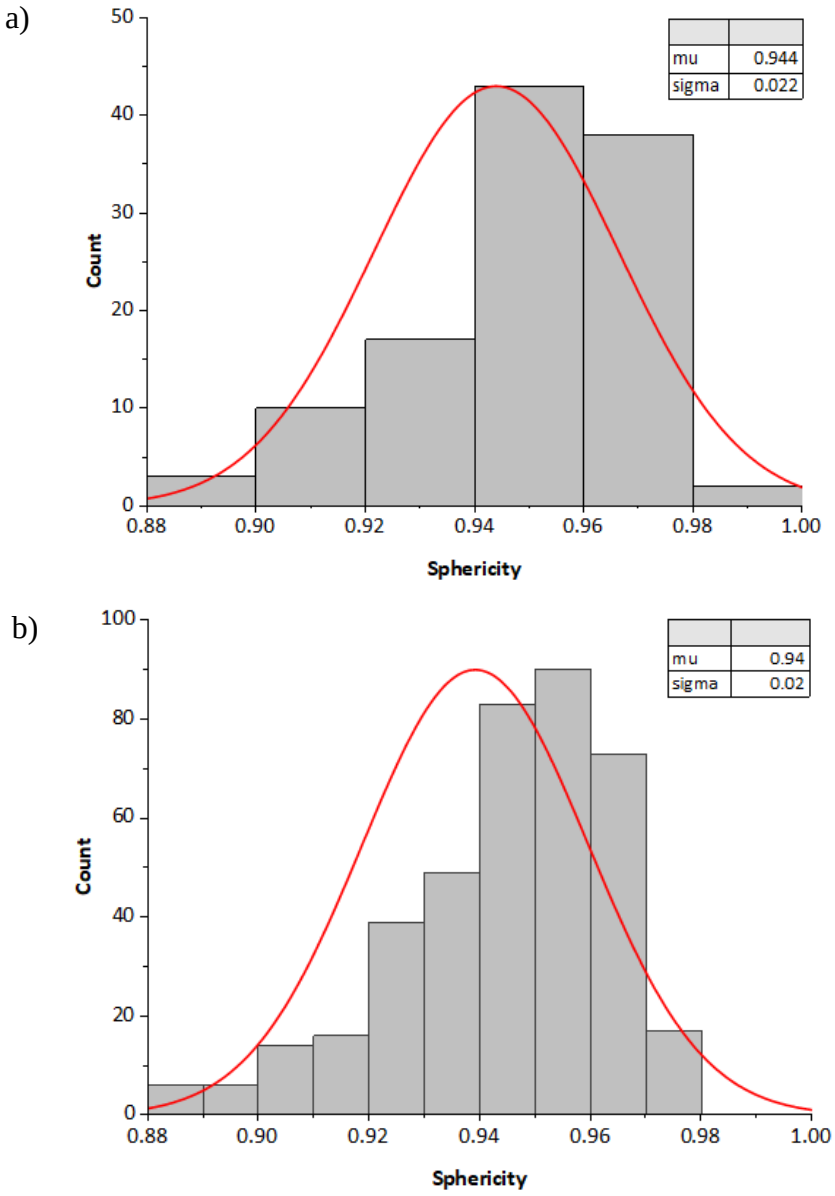

Fig 6. Pore sphericity distribution in a) as-built vertical and b) 1050 ℃- 1-hour heat treated vertical printed AM IN625 samples. Average and standard deviation are represented with mu and sigma values, respectively.

Pore sphericity within the as-built and 1050 ℃- 1-hour heat treated diagonally printed samples is presented in Figure 7. Similar observation was made in diagonally built samples compared to the vertically built samples. The average pore sphericity in the as-built and 1050 ℃- 1-hour heat treated diagonally built samples are 0.94 ± 0.2. In addition, from Figs. 6 and 7, it can be observed that the difference in the build orientation has a negligible effect on the average pore sphericity value.

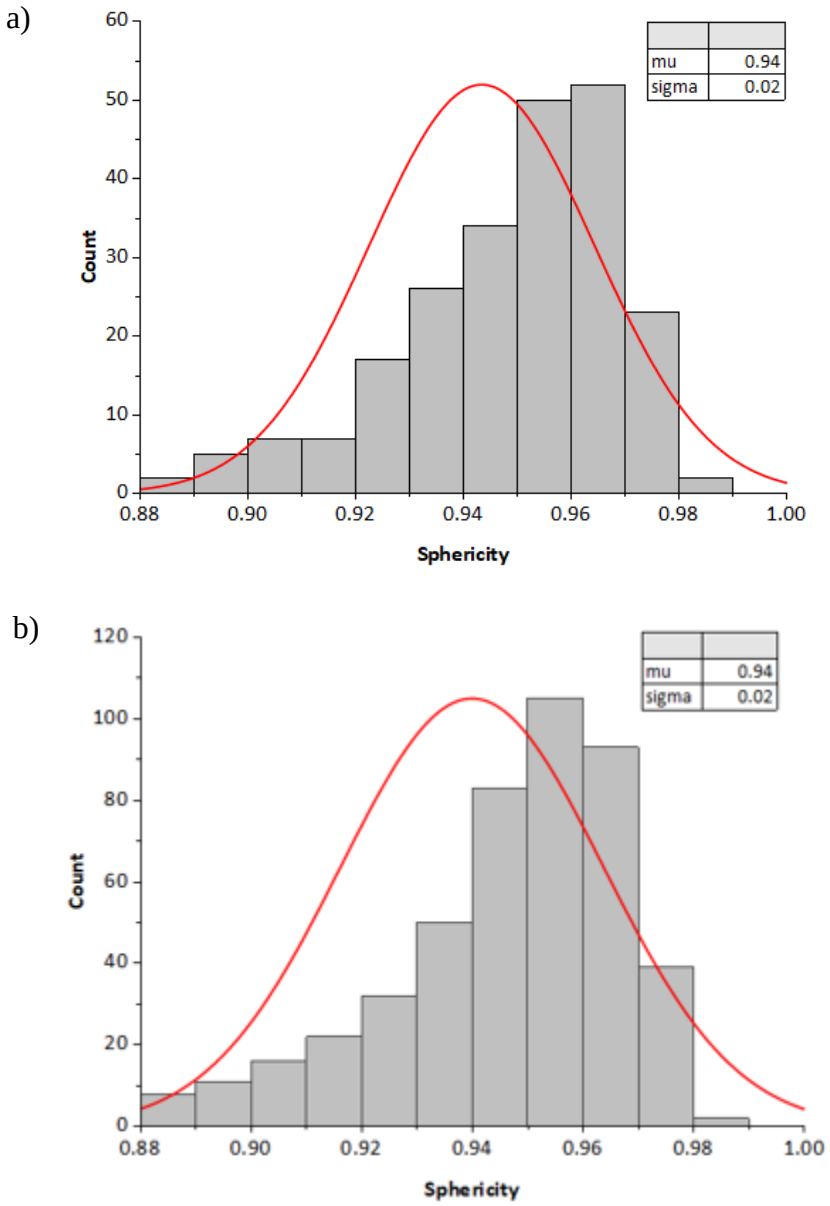

Fig 7. Pore sphericity distribution in a) as-built diagonal and b) 1050 ℃- 1-hour heat treated diagonal printed AM IN625 samples. Average and standard deviation are represented with mu and sigma values, respectively.

Conclusions

The present study investigated the effects of the build orientation and post processing heat treatment on the porosity characteristics in IN625 samples fabricated using laser powder bed fusion (L-PBF) additive manufacturing (AM). Samples were printed at vertical and diagonal orientation and used in as-built, and heat treated at 1050 ℃ for 1-hour conditions. Major conclusions are summarized as follows:

1. Build orientation and heat treatment had an influence on porosity count. The as-built vertical sample showed a lower porosity count compared to the as-built diagonal sample.

The as-built vertical sample had 186 pores compared to 367 pores in the as-built diagonal sample.

2. Heat treatment at 1050 ℃-1h, increased porosity count in both orientation-built samples. The 1050 ℃-1h heat treated vertical and diagonal samples had 1117 and 1389 porosity counts respectively.
3. Pores size increased in vertical and diagonal printed samples post 1050 ℃-1h heat treatment indicating the pressure increase in the pore.
4. However, neither build orientation nor heat treatment had a noticeable effect on the sphericity of pores in all samples. The average sphericity in all samples was observed to be 0.94.

Acknowledgements

This material is based upon work supported by the U.S. Department of Energy's Office of Nuclear Energy under Award Number DE-NE0008865.

References

[1] S. A. M. Tofail, E. P. Koumoulos, A. Bandyopadhyay, S. Bose, L. O'Donoghue, and C. Charitidis, "Additive manufacturing: scientific and technological challenges, market uptake and opportunities," *Materials Today*, vol. 21, no. 1, pp. 22–37, 2018, doi: https://doi.org/10.1016/j.mattod.2017.07.001.

[2] A. Mostafaei *et al.*, "Defects and anomalies in powder bed fusion metal additive manufacturing," *Current Opinion in Solid State and Materials Science*, vol. 26, no. 2, p. 100974, 2022, doi: https://doi.org/10.1016/j.cossms.2021.100974.

[3] ISO/ASTM 52900:2021(en), "Additive manufacturing — General principles — Fundamentals and vocabulary," *International Organization for Standardization*, p. 28, 2021.

[4] R. W. Cunningham, "Defect Formation Mechanisms in Powder-Bed Metal Additive Manufacturing," 2018, doi: 10.1184/R1/6715691.v1.

[5] W. H. Green, B. A. Cheeseman, D. M. Field, and K. R. Limmer, "Advanced X-ray Computed Tomography of Voids and Porosity in As-Cast FeMnAl Steel Alloy Material," no. ARL-TR-8975, 2020.

[6] A. du Plessis, "Effects of process parameters on porosity in laser powder bed fusion revealed by X-ray tomography," *Additive Manufacturing*, vol. 30, p. 100871, 2019, doi: https://doi.org/10.1016/j.addma.2019.100871.

[7] A. Du Plessis, "6 - Porosity in laser powder bed fusion," in *Fundamentals of Laser Powder Bed Fusion of Metals*, I. Yadroitsev, I. Yadroitsava, A. du Plessis, and E. MacDonald, Eds. Elsevier, 2021, pp. 155–178.

[8] H. Choo *et al.*, "Effect of laser power on defect, texture, and microstructure of a laser powder bed fusion processed 316L stainless steel," *Materials & Design*, vol. 164, p. 107534, 2019, doi: https://doi.org/10.1016/j.matdes.2018.12.006.

[9] J. B. Forien, J. D. Philip, G. M. Guss, B. H. Jared, J. D. Madison, and M. J. Matthews, "Effect of laser power on roughness and porosity in laser powder bed fusion of stainless

steel 316L alloys measured by X-ray tomography," *International Journal of Materials Research*, vol. 111, no. 1, pp. 47–54, 2020, doi: 10.3139/146.111816.

[10] P. Nandwana, M. M. Kirka, V. C. Paquit, S. Yoder, and R. R. Dehoff, "Correlations Between Powder Feedstock Quality, In Situ Porosity Detection, and Fatigue Behavior of Ti-6Al-4V Fabricated by Powder Bed Electron Beam Melting: A Step Towards Qualification," *Jom*, vol. 70, no. 9, pp. 1686–1691, 2018, doi: 10.1007/s11837-018-3034-6.

[11] G. Ziółkowski, E. Chlebus, P. Szymczyk, and J. Kurzac, "Application of X-ray CT method for discontinuity and porosity detection in 316L stainless steel parts produced with SLM technology," *Archives of Civil and Mechanical Engineering*, vol. 14, no. 4, pp. 608–614, 2014, doi: 10.1016/j.acme.2014.02.003.

[12] R. Zhao, A. Shmatok, R. Fischer, and B. C. Prorok, "Investigation of Causal Relationships between Printing Parameters, Pore Properties and Porosity in Laser Powder Bed Fusion," *Metals*, vol. 13, no. 2, 2023, doi: 10.3390/met13020330.

[13] M. Andurkar, B. Prorok, and S. M. . Thompson, "Effect of Build Orientation on Residual Stress and Microstructure in Inconel 625 Fabricated via Laser Powder Bed Fusion," 2022, doi: http://dx.doi.org/10.26153/tsw/44653.

[14] H. Bu, L. Chen, and Y. Duan, "Effect of Solution Heat Treatment on the Porosity Growth of Nickel-Based P/M Superalloys," *Metals*, vol. 12, no. 11, 2022, doi: 10.3390/met12111973.

[15] S. J. Hirsch, L. Winter, T. Grund, and T. Lampke, "Heat Treatment Influencing Porosity and Tensile Properties of Field Assisted Sintered AlSi7Mg0.6," *Materials*, vol. 15, no. 7, 2022, doi: 10.3390/ma15072503.